

INDI Control for the Oblique Wing-Quad Plane Drone

D.C. van Wijngaarden*, and B.D.W. Remes
Delft University of Technology, Kluyverweg 1, Delft

ABSTRACT

A type of UAV sharing the advantages of rotorcraft and fixed wing vehicles is the hybrid vehicle. Hybrid UAVs can take-off and land vertically and fly fast and efficient in forward flight due to the presence of a wing generating lift. However, combining the fixed wing and rotorcraft concept ends up in a multi-rotor with large dimensions when landed, and catching a lot of gust when hovering. Therefore, the oblique wing-quad plane drone has been developed which can rotate its quad arm and wing such that the wing can be aligned with the fuselage in hover. The wing can be rotated to fixed wing position during fast forward flight, stowing away one quad-arm. An INDI inner and outer loop controller has been implemented for this platform. Successful flight tests proved the feasibility of this controller and drone concept which is patent pending NL 2031701, Aeronautical Vehicle and Method of Transitioning between Flight Modes for an Aeronautical Vehicle, April 26th 2022,

1 INTRODUCTION

Since 2010 different VTOL-winged drones and control strategies are designed and integrated into different open-source autopilots, resulting in different VTOL-winged drone concepts. Merging multi-rotors and tail-sitters together, resulting in concepts like the Quadshot [1], ATMOS [2] and the NederDrone [3]. Merging a helicopter with a tail-sitter resulted in the DelftAcopter [4] and merging a fixed wing with a multi-rotor give the well know quad-plane concept [5]. Many more concepts have been designed but non of them are optimised for VTOL-winged flight and landing in a confined space like a drone-box.

This paper describes a new drone concept: The Oblique Wing-Quad Plane Drone which has the ability to vertically take-off and land, but the platform can skew its wing and quad arm in order to land in a confined space. During take-off and landing, the wing is directed parallel with the fuselage. While flying at higher airspeed, the wing and quad-arm can be rotated in-flight such that the hover motors will end up being rotated inside the fuselage and the wing being directed with its leading edge in the airflow. This way, a platform

can be optimised for forward flight while having the ability to take-off and land in the confined space of a drone-box.

An Incremental Non-linear Dynamic Inversion (INDI) controller is implemented for this drone as inner loop controller [6, 7]. No accurate model of the drone concept is needed for an INDI controller as the control method is sensor based and only actuator effectiveness values and dynamics are necessary to set-up a controller. Furthermore, the performance of disturbance rejection is high due to the direct angular acceleration feedback in the INDI controller. A Weighted Least Square (WLS) control allocation method has been applied to handle actuator saturation [8].

An INDI guidance controller has been derived for the outer loop as well. A similar INDI guidance method has already been proven to work well [9]. A WLS control allocation method was also been applied to the outer loop controller as the drone is over-actuated in pitch [5]. Therefore, a preferred pitch angle can be commanded within the saturation limits of the drone.

The architecture of the oblique wing-quad plane drone is outlined by section 2. The inner and outer loop INDI controllers applied to the drone are described by sections 3 and 4 respectively. A discussion on the results regarding experiments carried out with the drone are discussed in section 5. Finally, this paper end with a conclusion and recommendations for future research as given by section 6.

2 THE OBLIQUE WING-QUAD PLANE DRONE

The Drone-in-a-box concept is being deployed globally, making the drone sector more scalable than ever before. Operating VTOL-winged drones from a box implies limitations. They need a very large box, or they can only operate in low wind / no gust condition, as the wing introduce large disturbances in to the hovering platform due to wind gust.

When flying in fixed wing mode, the VTOL-winged drones actuators optimised for hover flight are often exposed to the free stream air, introducing parasitic drag during forward flight. An ideal VTOL-winged drone-in-a-box has no wing exposed during hover and has maximum multi-rotor control authority, while during cruise flight it has no hover actuators exposed and has a cruise speed optimised wing. Those conflicting demands resulting in the design of the oblique wing-quad plane drone. The drone takes-off, lands and hovers as a tailed quad-copter with an extra pusher propeller as depicted in figure 1. The skew angle Λ of the wing and the quad arm in this state is 0 degrees. When the airspeed increases, one quad arm rotates 90 deg around its midpoint inside the fuselage. While the wing which was aligned with the

*Email address: D.C.vanWijngaarden@tudelft.nl

fuselage during hover, rotates 90 deg, transforming the quad into an efficient fixed wing airplane with a dedicated forward propeller on its tail. The fixed wing state of the drone is given by figure 2. The skew angle Λ is set to 90 degrees in this state.

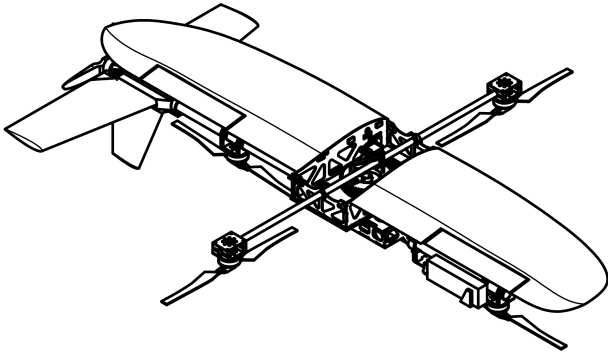


Figure 1: Oblique wing-quad plane with skew angle Λ set to 0 degrees.

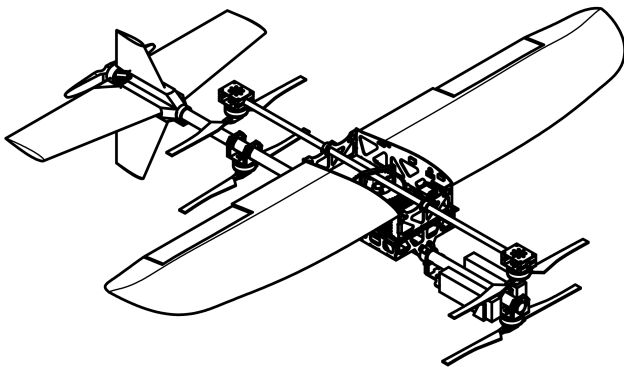


Figure 2: Oblique wing-quad plane with skew angle Λ set to 90 degrees.

The oblique wing-quad plane drone has a total of 10 actuators to control its attitude, linear accelerations and the skew angle of the rotating wing and quad arm. The drone has 5 motors, 4 control surfaces and one servo to rotate one quad arm and the wing. Figure 3 shows a graphical representation of the drone for which the wing is skewed halfway. Each actuator is numbered in the figure and described by table 1 accordingly. The right column of the table shows whether the actuator is rotating with skew angle.

To maximise control authority of the vehicle during hover, fixed wing and transition, a dedicated Incremental Non linear Dynamic Inversion controller (INDI) is designed as described by the next sections in this paper.

3 INDI INNER LOOP CONTROL AND SCHEDULING

The attitude control approach that has been implemented on the rotating wing drone is based on Incremental Nonlin-

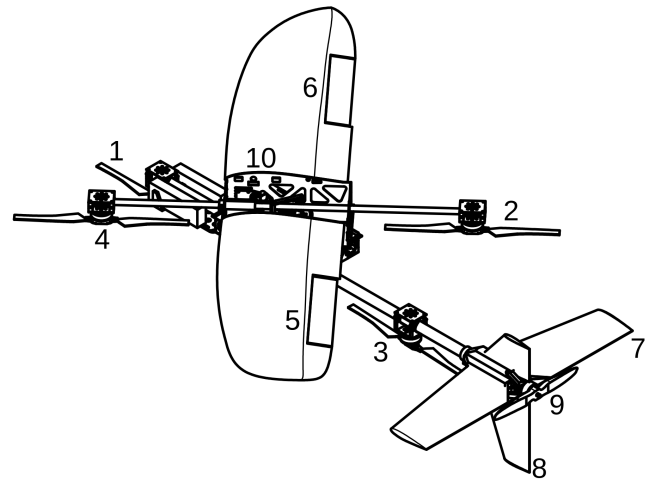


Figure 3: Actuator schematic of the oblique wing-quad plane drone.

Actuator number	Actuator name	Rotating
1	front motor	
2	right motor	✓
3	back motor	
4	left motor	✓
5	left aileron	✓
6	right aileron	✓
7	elevator	
8	rudder	
9	push motor	
10	wing rotation servo	

Table 1: List of actuators for the oblique wing-quad plane drone.

ear Dynamic Inversion (INDI) as outlined by [6]. A weighted least square (WLS) control allocation method has been implemented to the INDI attitude controller to prioritise the control of a certain control axis in case of actuator saturation [8]. The WLS method can also prefer the use aerodynamic surfaces over motors to stabilise the drone.

The implemented INDI controller is based on the second law of Newton:

$$\ddot{\xi} = g + m^{-1} (M_{NB} f + f_{ext}) \quad (1)$$

where ξ denotes the position vector in the North East Down (NED) reference frame and g the gravitational acceleration in the same reference frame. The value of m is the mass of the drone. The force vector f is the input force in the body reference frame due to changes in thrust level and attitude. M_{NB} is the rotation matrix from the body frame to the NED reference frame. The matrix is obtained from the at-

titude quaternion q . Finally, vector f_{ext} contains the external unmodeled forces acting on the system.

The equation of rotational dynamics of the system is given by:

$$\dot{\Omega} = J^{-1}(m + m_{ext} - \Omega \times J\Omega), \quad (2)$$

where Ω is the attitude vector containing the roll, pitch and yaw angle respectively. The vector J is the vehicle's mass moment of inertia in the body reference frame. The vectors m and m_{ext} represent the moments generated by control inputs and unmodeled external disturbances respectively.

It can be approximated that the change in angular acceleration of the system is induced due to a change in input vector u by neglecting cross terms in the inertia matrix J :

$$\dot{\Omega} - \dot{\Omega}_0 = G_1(u - u_0) + G_2(\dot{u} - \dot{u}_0), \quad (3)$$

where G_1 is the control effectiveness matrix and G_2 is the control effectiveness with respect to the derivative of the control input vector u .

The first 8 actuators given in table 1 can manipulate the angular accelerations as given by Ω . Therefore, the INDI inner loop controls those 8 actuators and therefore the control input vector u consist of 8 entries. As a result, the effectiveness matrices G_1 and G_2 consists of 8 columns and 3 rows. The effectiveness matrix G_1 is build up as follows:

$$G_1 = [G_{1_1} \ G_{1_2} \ G_{1_3} \ G_{1_4} \ G_{1_5} \ G_{1_6} \ G_{1_7} \ G_{1_8}] \quad (4)$$

In the first place, control effectiveness values need to be scheduled with the drone's skew angle Λ as some actuators are moving with changing skew angle as shown by table 1. This scheduling is applied to the side-motors and ailerons. A 3D CAD model shows the roll and pitch moments of inertia only marginally change by changing the skew angle. Therefore, the pitch and roll control effectiveness values of the side motors and ailerons can be scheduled with trigonometric functions of the skew angle Λ .

Secondly, the control effectiveness of aerodynamic surfaces are scheduled with dynamic pressure. Those effectiveness values are therefore dependent on the airspeed squared. Airspeed is measured by a pitot tube directed in the body x axis.

The first column of the effectiveness matrix G_1 corresponds to the front motor which can control angular pitch and yaw accelerations as shown by the following:

$$G_{1_1} = [0 \ g_{1_{21}} \ g_{1_{31}}]^T \quad (5)$$

The second column of the control effectiveness matrix corresponds to the right motor for which roll and pitch effectiveness is scheduled by the cosine and sine of the skew angle Λ respectively. The roll effectiveness was determined for a skew angle Λ of 0 degrees, quad-mode, and subsequently

scheduled by scaling it with the cosine of the skew angle. On the contrary, the pitch effectiveness has been determined for the fixed wing state with skew angle Λ set to 90 degrees and thereafter scheduled by scaling this value with the sine of the skew angle as shown below:

$$G_{1_2} = [g_{1_{12}}^{\Lambda=0} c\Lambda \ g_{1_{22}}^{\Lambda=\pi/2} s\Lambda \ g_{1_{32}}]^T \quad (6)$$

The third column of the effectiveness matrix corresponds to the back motor which is equivalent to the front motor except the sign of the pitch effectiveness value:

$$G_{1_3} = [0 \ g_{1_{23}} \ g_{1_{33}}]^T \quad (7)$$

The control effectiveness scheduling of the left motor is equivalent to the right motor except the signs of the roll and pitch effectiveness values air opposite. The fourth column of the control effectiveness matrix corresponding to this motor is given below:

$$G_{1_4} = [g_{1_{14}}^{\Lambda=0} c\Lambda \ g_{1_{24}}^{\Lambda=\pi/2} s\Lambda \ g_{1_{34}}]^T \quad (8)$$

The roll and pitch effectiveness of the left and right ailerons can be scheduled by sine and cosine functions based on the skew angle Λ as those control surfaces are being displaced by changing the skew angle. In the current research stage, the control effectiveness values of the ailerons in pitch $g_{1_{25}}$ and $g_{1_{26}}$ have not yet been defined and set to 0 such that the ailerons will only handle roll control. The roll effectiveness values $g_{1_{15}}^{\Lambda=\pi/2}$ and $g_{1_{16}}^{\Lambda=\pi/2}$ have been defined in fixed wing state and scheduled by airspeed squared. The effectiveness columns in effectiveness matrix G_1 of the left and right ailerons are defined by the following two equations respectively:

$$G_{1_5} = [g_{1_{15}}^{\Lambda=\pi/2} (V^2) s\Lambda \ g_{1_{25}}^{\Lambda=0} (V^2) c\Lambda \ 0]^T \quad (9)$$

$$G_{1_6} = [g_{1_{16}}^{\Lambda=\pi/2} (V^2) s\Lambda \ g_{1_{26}}^{\Lambda=0} (V^2) c\Lambda \ 0]^T \quad (10)$$

The elevator effectiveness corresponds to the the seventh column and is only effective in pitch. As this actuator is a control surface, it is aerodynamically being scheduled by airspeed squared as shown below:

$$G_{1_7} = [0 \ g_{1_{27}} (V^2) \ 0]^T \quad (11)$$

Finally, the last column of the effectiveness matrix corresponds to the rudder. The surface is only effective in yaw and scheduled with airspeed squared:

$$G_{1_8} = [0 \ 0 \ g_{1_{38}} (V^2)]^T \quad (12)$$

For the G_2 effectiveness matrix it is assumed that only the first four actuators (hover motors) generate a moment in yaw with respect to the derivative of the control input vector \mathbf{u} .

For INDI control, equation 3 should be discretized and subsequently inverted in order to compute the control input vector \mathbf{u} at every time step of the control loop. The values of the angular accelerations $\dot{\Omega}_0$ can be obtained by differentiation of the onboard gyroscope reading. Due to the presence of high frequency vibrations, a low-pass filter is applied to the angular accelerations denoted by subscript f. The control input vector \mathbf{u}_0 is filtered by the same low-pass filter in order to synchronise the input with the filtered angular acceleration signal. The value of $\dot{\mathbf{u}}$ can be approximated using the unit delay operator L . A prediction of the angular accelerations $\dot{\Omega}$ can be made based on a new control input command \mathbf{u}_c :

$$\dot{\Omega} - \dot{\Omega}_f = (\mathbf{G}_1 + \mathbf{G}_2)(\mathbf{u}_c - \mathbf{u}_f) + \mathbf{G}_2 L(\mathbf{u}_c - \mathbf{u}_f). \quad (13)$$

In order to compute the control input \mathbf{u}_c , the equation can be inverted by a pseudo inverse. However, the pseudo inverse of the effectiveness matrices is non singular due to the over-actuated characteristic of the oblique wing-quad plane drone. For that reason, a sophisticated Weighted Least Square (WLS) control allocation method is applied to the inner loop [8]. Inverting equation 13 yields:

$$\mathbf{u}_c = \mathbf{u}_f + (\mathbf{G}_1 + \mathbf{G}_2)^+(\boldsymbol{\nu} - \dot{\Omega}_f + \mathbf{G}_2 z^{-1}(\mathbf{u}_c - \mathbf{u}_f)) \quad (14)$$

Where the $(\cdot)^+$ denotes the inverse which is being handled by the applied WLS method. The vector $\boldsymbol{\nu}$ reference angular accelerations that are simply be calculated using a PD controller. Due to direct feedback of the angular accelerations by differentiating the gyroscope, disturbances can be counteracted fast [6, 7].

4 INDI OUTER LOOP CONTROL

The INDI outer loop controller of the oblique wing-quad plane drone provides the method for guidance for the platform. Derivations of an INDI outer loop controller for multiple types of drones is described by [9, 10]. For over-actuated systems such as the oblique wing-quad plane, a control allocation method can be applied on the outer loop as applied in [5].

The outer loop INDI controller is based on the second law of Newton as shown below:

$$\ddot{\boldsymbol{\xi}} = \mathbf{g} + \frac{1}{m} \mathbf{L}_N(\boldsymbol{\eta}, V, \Lambda) + \frac{1}{m} \mathbf{D}_N(\boldsymbol{\eta}, V, \Lambda) + \frac{1}{m} \mathbf{T}_N(\boldsymbol{\eta}, T) \quad (15)$$

The vector $\ddot{\boldsymbol{\xi}}$ consists of the vehicle's accelerations in the NED reference system. The vector \mathbf{g} is the gravitational acceleration which is directed downwards. The vectors \mathbf{L}_N ,

\mathbf{D}_N and \mathbf{T}_N represent the lift, drag and thrust forces in the NED reference frame respectively. Vector $\boldsymbol{\eta}$ represents the attitude in ZXY rotation order ($\boldsymbol{\eta} = [\psi \ \phi \ \theta]^T$). The lift and drag in the NED frame are dependent on attitude, velocity and skew angle. The thrust force in this frame of reference is dependent on attitude and thrust input to the hover motors and pusher motor.

In order to transform forces generated in the body reference frame to the NED reference frame, the following rotation matrix in ZXY rotation order has been derived:

$$\mathbf{M}_{NB} = \begin{bmatrix} c\theta c\psi - s\phi s\theta s\psi & -c\phi s\psi & s\theta c\psi + s\phi c\theta s\psi \\ c\theta s\psi + s\phi s\theta c\psi & c\phi c\psi & s\theta s\psi - s\phi c\theta c\psi \\ -c\phi s\theta & s\phi & c\phi c\theta \end{bmatrix} \quad (16)$$

Thrust of the oblique wing-quad plane drone can be generated in two directions in the body frame. The hover props can generate thrust in the negative Z direction (T_{B_z}) using the hover motors and positive thrust in the X direction using the pusher motor (T_{B_x}) as shown below:

$$\mathbf{T}_B = [T_{B_x} \ 0 \ T_{B_z}]^T \quad (17)$$

Rotating the body thrust vector \mathbf{T}_B to the NED reference system in ZXY order yields the vector \mathbf{T}_N :

$$\mathbf{T}_N = \begin{bmatrix} (c\theta c\psi - s\phi s\theta s\psi)T_{B_x} + (s\theta c\psi + s\phi c\theta s\psi)T_{B_z} \\ (c\theta s\psi + s\phi s\theta c\psi)T_{B_x} + (s\theta s\psi - s\phi c\theta c\psi)T_{B_z} \\ -c\phi s\theta T_{B_x} + c\phi c\theta T_{B_z} \end{bmatrix} \quad (18)$$

The lift force in the body reference frame is directed in the negative Z direction and is dependent on the pitch angle, velocity and skew angle. Assuming small flight path angles, lift can be linearized around a zero pitch angle. Converting the lift to the NED reference system yields \mathbf{L}_N :

$$\mathbf{L}_N = \mathbf{M}_{NB}^{\theta=0} \mathbf{L}_B(\theta, V, \Lambda) = \begin{bmatrix} s\phi s\psi L(\theta, V, \Lambda) \\ -s\phi c\psi L(\theta, V, \Lambda) \\ c\phi L(\theta, V, \Lambda) \end{bmatrix} \quad (19)$$

It is assumed that the drag forces changes slowly with respect to thrust and lift such that the influence on the change in acceleration can be neglected. This means that only thrust and lift forces need to be evaluated for the construction of the outer loop effectiveness matrix. This also means that for straight and level flight at constant speed, the value of $T_{b_x} = 0$ as T_{b_x} is the only modelled force in the body X axis.

An incremental model can be derived using a first order Taylor expansion. This can be done by taking partial derivatives with respect to the controlled input variables ($\mathbf{v} = [\phi \ \theta \ a_{B_z} \ a_{B_x}]^T$) as shown in the below equation:

$$\ddot{\boldsymbol{\xi}} = \ddot{\boldsymbol{\xi}}_0 + \frac{1}{m} (\mathbf{G}_T(\boldsymbol{\eta}, T) + \mathbf{G}_L(\boldsymbol{\eta}, V, \Lambda)) (\mathbf{v} - \mathbf{v}_0), \quad (20)$$

The linear accelerations $\ddot{\xi}_0$ are being measured by the drone's accelerometer. As this sensor also measures high frequency vibrations, this signal should be filtered using a low-pass filter resulting in the filtered acceleration vector $\ddot{\xi}_f$ subscripted with f. Vector v_0 is also filtered with the same low-pass filter in order to synchronise the signals of the filtered accelerometer $\ddot{\xi}_f$ with the controlled input variables. After that, the equation can be inverted to obtain:

$$v = v_f + m(G_T(\eta, T) + G_L(\eta, V, \Lambda))^{-1} (\ddot{\xi}_{\text{ref}} - \ddot{\xi}_f) \quad (21)$$

where $\ddot{\xi}_{\text{ref}}$ is the reference acceleration to track which is being generated using a PD loop.

The control effectiveness matrices for thrust and lift are given by:

$$G_T(\eta, T_{Bx}, T_{Bz}) = \begin{bmatrix} \left(\frac{\partial}{\partial \phi} \frac{1}{m} \mathbf{T}_N(\phi, \theta_0, \psi_0, T_{Bz0}, T_{Bx0}) \Big|_{\phi=\phi_0} \right)^T \\ \left(\frac{\partial}{\partial \theta} \frac{1}{m} \mathbf{T}_N(\phi_0, \theta, \psi_0, T_{Bz0}, T_{Bx0}) \Big|_{\theta=\theta_0} \right)^T \\ \left(\frac{\partial}{\partial T_{Bz}} \frac{1}{m} \mathbf{T}_N(\phi_0, \theta_0, \psi_0, T_{Bz}, T_{Bx0}) \Big|_{T_{Bz}=T_{Bz0}} \right)^T \\ \left(\frac{\partial}{\partial T_{Bx}} \frac{1}{m} \mathbf{T}_N(\phi_0, \theta_0, \psi_0, T_{Bz0}, T_{Bx}) \Big|_{T_{Bx}=T_{Bx0}} \right)^T \end{bmatrix}^T \quad (22)$$

and

$$G_L(\eta, V, \Lambda) = \begin{bmatrix} \left(\frac{\partial}{\partial \phi} \frac{1}{m} \mathbf{L}_N(\phi, \theta_0, \psi_0, V_0, \Lambda_0) \Big|_{\phi=\phi_0} \right)^T \\ \left(\frac{\partial}{\partial \theta} \frac{1}{m} \mathbf{L}_N(\phi_0, \theta, \psi_0, V_0, \Lambda_0) \Big|_{\theta=\theta_0} \right)^T \\ \mathbf{0}^T \\ \mathbf{0}^T \end{bmatrix}^T \quad (23)$$

Further elaborating those effectiveness functions result in:

$$G_T(\eta, T_{Bx}, T_{Bz}) = \frac{T_{bz}}{m} \begin{bmatrix} c\phi c\theta s\psi & c\theta c\psi - s\psi s\theta s\psi & 0 & 0 \\ -c\phi c\theta c\psi & c\theta s\psi + s\phi s\theta c\psi & 0 & 0 \\ -s\phi c\theta & -c\phi s\theta & 0 & 0 \end{bmatrix} + \frac{1}{m} \begin{bmatrix} 0 & 0 & s\theta c\psi + s\phi c\theta s\psi & c\theta c\psi - s\phi s\theta s\psi \\ 0 & 0 & s\theta s\psi - s\phi c\theta c\psi & c\theta s\psi + s\phi s\theta c\psi \\ 0 & 0 & c\phi c\theta & -c\phi s\theta \end{bmatrix} \quad (24)$$

and

$$G_L(\eta, V, \Lambda) = \frac{1}{m} \begin{bmatrix} c\phi s\psi L(\theta, V, \Lambda) & s\phi s\psi \frac{\partial}{\partial \theta} L(\theta, V, \Lambda) & 0 & 0 \\ -c\phi c\psi L(\theta, V, \Lambda) & -c\psi s\phi \frac{\partial}{\partial \theta} L(\theta, V, \Lambda) & 0 & 0 \\ -s\phi L(\theta, V, \Lambda) & c\phi \frac{\partial}{\partial \theta} L(\theta, V, \Lambda) & 0 & 0 \end{bmatrix} \quad (25)$$

The functions $L(\theta, V)$ and $\frac{\partial}{\partial \theta} L(\theta, V)$ still have to be defined for the vehicles with a wing, for a pure rotorcraft they are zero. Recognizing that the lift and T_{Bz} only need to be known to compute the effectiveness of rolling, we assume level flight and a simple relationship with the pitch angle:

$$L(\theta, V, \Lambda) + T_{Bz}(\theta) \approx L(\theta, \Lambda) + T_{Bz}(\theta) = -9.81m \quad (26)$$

For experiments that have been performed, the reference of the yaw angle ψ was set in direction of a windtunnel duct.

Because the pseudo inverse of the outer loop effectiveness matrix is non-singular, a Weighted Least Square (WLS) control allocation method has been applied to calculate the virtual control vector v [8, 5]. As the UAS is over-actuated in pitch, a preferred pitch angle within the saturation limits of the vehicle can be controlled using this control allocation scheme.

5 TEST RESULTS

A transition flight test was performed with the oblique wing-quad plane drone in order to show the working principles of the INDI inner and outer loops and show the feasibility of the design. The tests have been performed in the Open Jet Facility (OJF) of Delft University of Technology [11]. The OJF is a windtunnel facility with a cross section of about 2 by 2 meters. The facility can generate wind speeds up to 35 m/s. The test section is big enough to fly the oblique wing-quad plane drone within the facility to verify the inner and outer loop controllers. The drone is being tracked by an opti-track system and tethered to the ceiling with a rope for safety. The force is being released from the safety rope during flight in order to mimic real flight characteristics. The position accuracy of the vehicle was appropriate to keep it in the test section of the windtunnel during the experiments.

A hover to forward and back to hover transition flight has been performed in the windtunnel. This is done by starting the drone with 0 skew angle in the windtunnel and let it hover autonomous at a fixed position. Photographs of the of a transition from hover to forward flight are given by figure 4. The top image corresponds to hover flight, the middle image to transition flight and the bottom image to forward flight. An airflow of 17 m/s is being generated when the windtunnel is spinned up. This airflow is measured by the pitot tube of the drone as plotted by figure 5. It can be seen from the plot that the airflow is first being increased and at the end of the experiment being decreased.

in order to have a stable hover flight, the drone starts at a 0 skew angle, but the skew angle is automatically being increased to 90 degrees when higher airspeed is being measured. This is done to transform the drone from a quad into a fixed wing to generate lift with its wings with increasing airspeed. A plot of the skew angle over time is given by figure 6. It can be clearly seen when comparing the plot to the airspeed plot that the skew angle is changing with airspeed.

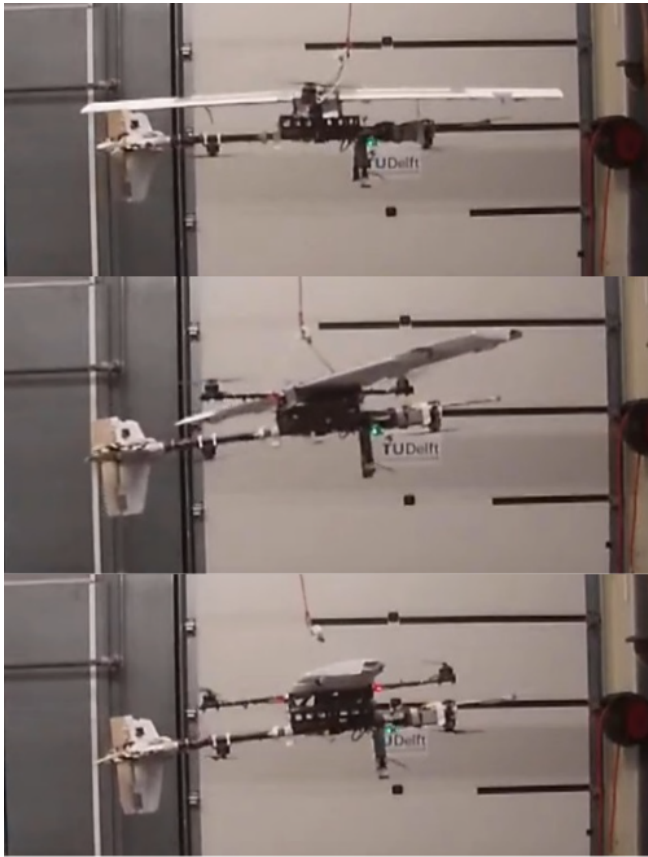


Figure 4: Transition of oblique wing-quad plane drone hover to forward flight.

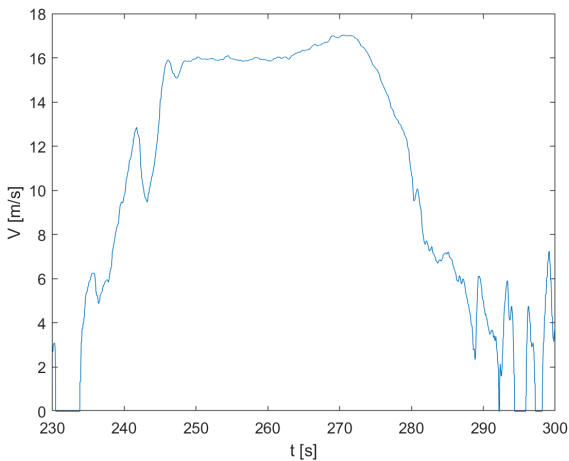


Figure 5: Airspeed versus time during hover-forward-hover transition flight.

Another phenomenon that could be observed from the experiment is the exchange of lift from its hover props (motor 1 to 4) to its wing by looking at the thrust level over time

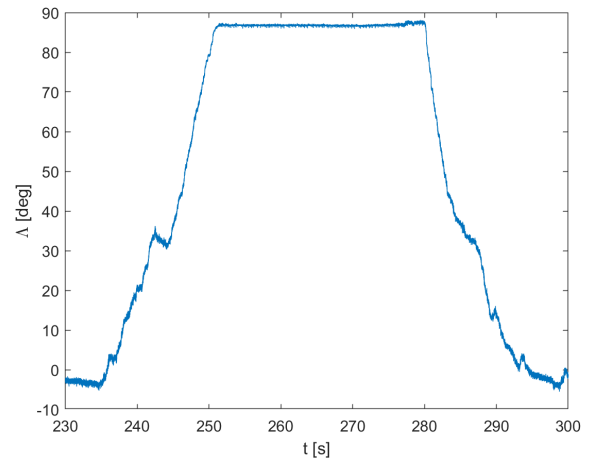


Figure 6: Skew angle versus time during hover-forward-hover transition flight.

plot given by figure 7. The blue line corresponds to the hover motors and it can be clearly seen that thrust is being reduced when airspeed is being increased. On the other hand, the orange line shows that the thrust on the pusher motor is being increased with airspeed as more thrust along the drone's longitudinal axis is required to keep its position in the windtunnel.

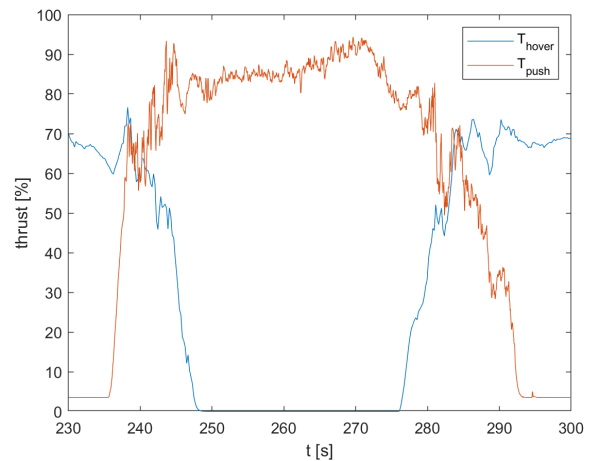


Figure 7: Thrust level versus time during hover-forward-hover transition flight.

The attitude of the drone during the transition test is shown in figure 8. The plot shows the measured and reference angles in blue and orange respectively. From the top and bottom plots, it can be seen that the roll and yaw angles oscillate a little at t=240s and t=280s. This corresponds to a state where the skew angle Δ is set to about 30-45 degrees at an airspeed of about 7-8 m/s. The control authority of the

http://www.imavs.org/

drone is reduced within this speed regime due to the following phenomena: the back hover motor is blowing air downwards in the vicinity of the elevator. This causes a downward flow of air over the elevator resulting in a negative angle of attack. Therefore, the elevator need to be deflected fully downward up to saturation after which the hover motors saturate in pitch. Due to coupling between the roll, pitch and yaw, this saturation can be seen on other axes as well. This is not a problem for higher airspeed because the thrust generated by the hover motors will gradually go down and the pitch effectiveness of the elevator increases.

Another characteristic of the drone that can be observed from figures 5 to 9 is that the vehicle can fly in fixed wing configuration, even below stall speed, with a skew angle of 90 degrees where upward forces are generated by both the hover motors and wing lift. This can be clearly observed in the time frame running from 275 to 285 seconds. The speed of the airflow is gradually being reduced within this time frame in which the drone starts in fixed wing mode with hover props switched off as can be seen in figure 7. From figure 8 can be observed that first the pitch is being increased after which the hover motors are switched on when the maximum pitch angle has been reached. In this low speed fixed wing state, the hover motors and lift keep the drone up in the air below the stall speed of the fixed wing configuration. It can be observed that from $t = 283s$ the airspeed drops below 8 m/s and only then the wing start to skew back to quad mode as shown in figure 6.

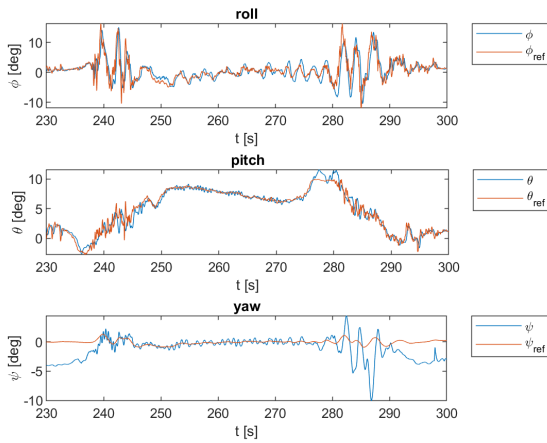


Figure 8: Attitude versus time during hover-forward-hover transition flight.

Finally, a plot of the tracked position and reference position is given by figure 9. It shows the tracked positions with blue lines and reference positions with orange lines. it can be seen that the position error increases for the same time periods as where roll and yaw oscillations occur. The position errors were small enough to keep the drone during its flight

within the test section of the windtunnel without putting any tension on the safety rope.

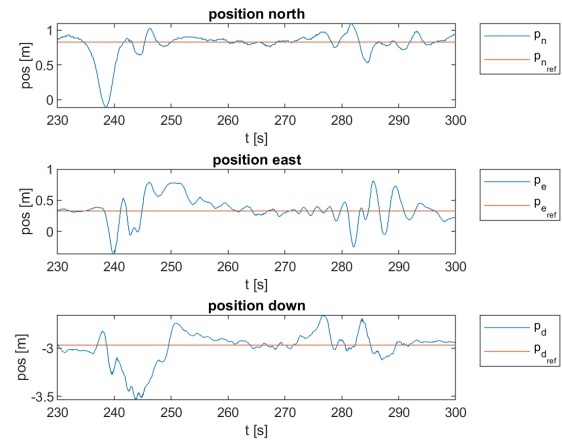


Figure 9: Position versus time during hover-forward-hover transition flight.

6 CONCLUSIONS AND RECOMMENDATIONS

This paper described the design of the new oblique wing-quad plane drone. It was shown that using the current implemented controller a free flight transition from quad to fixed wing and back could be performed within the 2x2m limits of the test section of the OJF (Open jet windtunnel Facility). We can conclude that the design oblique wing-quad plane is feasible of performing transition in flight within a variety of airspeeds.

The design of the drone can be updated in the future to solve the pitch saturation that occurs around 7-8 m/s airspeed. Also more tests can be performed outdoors and in the wind-tunnel to be able to model the drone better in order to improve the tuning and effectiveness scheduling of the INDi inner and outer loop control methods. Like the change of the effectiveness of the hover propellers with changing airspeed. Furthermore, an aerodynamic fuselage should be designed to make the drone more efficient in forward flight.

REFERENCES

- [1] P. Sinha, P. Esden-Tempski, C.A. Forrette, J.K. Gibboney, and G.M. Horn. Versatile, modular, extensible vtol aerial platform with autonomous flight mode transitions. pages 1–17, 03 2012.
- [2] C. De Wagter, D. Dokter, G.C.H.E. Croon, and B.D.W. Remes. Multi-lifting-device uav autonomous flight at any transition percentage. 01 2013.
- [3] C. De Wagter, B.D.W. Remes, R. Ruijsink, F. van Tienen, and E. van der Horst. Design and testing of a vertical take-off and landing uav optimized for carrying

http://www.imavs.org/

a hydrogen fuel cell with a pressure tank. *Unmanned Systems*, 08(04):279–285, 2020.

- [4] C. De Wager, B.D.W. Remes, R. Ruijsink, E. Van Der Horst, F. Van Tienen, D.C. Van Wijngaarden, J. Meulenbeld, and K. Van Hecke. DelftaCopter Propulsion Optimization from Hover to Fast Forward Flight using Windtunnel Measurements. *IMAV 2018: International Micro Air Vehicle Conference and Competition 2018*, November:30–38, 2018.
- [5] H J Karssies and C. De Wagter. XINCA : Extended Incremental Non-linear Control Allocation on a Quadplane. *IMAV 2021: International Micro Air Vehicle Conference and Competition 2021*, pages 74–84, 2021.
- [6] E.J.J. Smeur, Q. Chu, and G.C.H.E. De Croon. Adaptive incremental nonlinear dynamic inversion for attitude control of micro air vehicles. *Journal of Guidance, Control, and Dynamics*, 39(3):450–461, 2016.
- [7] Ewoud J. J. Smeur, G.C.H.E. de Croon, and Q. Chu. Cascaded incremental nonlinear dynamic inversion for MAV disturbance rejection. *Control Engineering Practice*, 73:79–90, apr 2018.
- [8] E.J.J. Smeur, D.C. Höppener, and C. De Wagter. Prioritized Control Allocation for Quadrotors Subject to Saturation. *IMAV 2017: International Micro Air Vehicle Conference and Competition 2017*, (September):37–43, 2017.
- [9] D.C. Van Wijngaarden, E.J.J. Smeur, and B.D.W. Remes. Flight Code Convergence : Fixedwing , Rotorcraft , Hybrid. *IMAV 2021: International Micro Air Vehicle Conference and Competition 2021*, September:21–27, 2021.
- [10] E.J.J. Smeur, M. Bronz, and G.C.H.E. de Croon. Incremental control and guidance of hybrid aircraft applied to a tailsitter unmanned air vehicle. *Journal of Guidance, Control, and Dynamics*, 43(2):274–287, 2020.
- [11] Open jet facility. <https://www.tudelft.nl/lr/organisatie/afdelingen/aerodynamics-wind-energy-flight-performance-and-propulsion/facilities/low-speed-wind-tunnels/open-jet-facility>. Accessed: 2022-05-29.